Journal of Environmental Management 413 (2026) 130358

Contents lists available at ScienceDirect

Journal of Environmental Management

journal homepage: www.elsevier.com/locate/jenvman

Research article

Heatwave-driven amplification of ozone formation offsets emission control benefits in VOC-limited megacities

Han-Jun Ji [a], Hyo-Jung Lee [a,b], Jong-Min Kim [a], Sang-Seok Oh [a], Min-Seong Kim [a], Cheol-Hee Kim [a,b,*]

[a] Department of Atmospheric Sciences, Pusan National University, Busan, 46241, Republic of Korea
[b] Institute of Environmental Studies, Pusan National University, Busan, 46241, Republic of Korea

ARTICLE INFO

Handling Editor: Jason Michael Evans

Keywords:
Ozone formation
Heatwave
Biogenic volatile organic compounds (BVOCs)
Climate change penalty
VOC-limited regime

ABSTRACT

Amid an ongoing warming climate, long-term increases in surface ozone (O_3) concentrations have been reported across East Asia, including South Korea, despite sustained efforts to reduce precursor emissions. In this study, we use an extreme heat episode as a physically plausible analog of near-future warming conditions to examine how climate-driven temperature increases may offset the air quality benefits of emission reductions in two major metropolitan areas in South Korea: Seoul and Busan. Specifically, we selected the unprecedented heatwave during the summer of 2018, which recorded the highest seasonal mean temperature over the past decade and represents meteorological conditions analogous to those expected under continued climate warming. Heatwave-specific biogenic volatile organic compound (BVOC) emissions were contrasted with those during non-heatwave conditions using surface observations, satellite-based formaldehyde (HCHO) retrievals from TROPOMI, and WRF-Chem simulations. The results show that temperature was positively correlated with both HCHO and O_3 in Seoul ($R = 0.59$ and 0.69, respectively) and Busan ($R = 0.60$ and 0.57, respectively), consistent with enhanced temperature-driven BVOC emissions and subsequent oxidation reflected by HCHO. These findings indicate that rising temperatures intensify photochemical reactions and alter O_3 production sensitivity in major megacities through the amplification of BVOC emissions, particularly under VOC-limited ozone formation regimes. Our results suggest that continued climate warming, represented here by historically observed extreme heat conditions, may impose a climate change penalty on urban ozone, implying that substantially greater emission reductions will be required to attain equivalent air quality benefits in major East Asian cities under future warming.

1. Introduction

Ozone (O_3) is a secondary pollutant formed through nonlinear photochemical reactions involving nitrogen oxides (NO_x) and reactive carbon species, including methane (CH_4), carbon monoxide (CO), and non-methane volatile organic compounds (NMVOCs), under solar radiation. High-O_3 episodes are influenced not only by precursor emissions but also by meteorological and climatological conditions—such as temperature, radiation, and atmospheric stagnation—that play critical roles in ozone formation. Despite ongoing emission-control policies that have reduced anthropogenic precursor emissions, surface O_3 concentrations have continued to increase in megacities across East Asia (Lee et al., 2021, 2022). More specifically, observations over the Seoul Metropolitan Area showed decreasing NO_2 concentrations during 2015–2019 despite increasing surface O_3 concentrations (Colombi et al., 2023). A subsequent nationwide analysis for 2015–2023 also reported persistent decreases in surface NO_2, together with increases in high-percentile O_3, particularly in the Seoul Metropolitan Area (Oak et al., 2025). Given the substantial health and economic impacts associated with air pollution in rapidly urbanizing regions of East Asia, understanding the factors that offset air-quality improvements remains an important scientific and policy challenge (Ding et al., 2025; Jin et al., 2025).

Climate change is expected to further increase surface temperatures, making heat-related effects increasingly relevant to air quality. The Sixth Assessment Report of the Intergovernmental Panel on Climate Change (IPCC AR6) indicates that the global mean temperature has already increased by approximately 1.1 °C relative to the pre-industrial

* Corresponding author. Department of Atmospheric Sciences, Pusan National University, 2 Busandaehak-ro 63beon-gil, Geumjeong-gu, Busan, 46241, Republic of Korea.
E-mail address: chkim2@pusan.ac.kr (C.-H. Kim).

https://doi.org/10.1016/j.jenvman.2026.130358
Received 5 March 2026; Received in revised form 24 June 2026; Accepted 27 June 2026
Available online 1 July 2026

period and projects that, if warming exceeds 1.5–2.0 °C, the frequency and intensity of extreme heat events will increase substantially (IPCC, 2021). As temperature is a key meteorological driver of ozone formation, climate-induced warming is likely to influence future air quality. Climate projections therefore provide an important framework for assessing the contribution of warming to changes in ozone pollution.

Air temperature exerts a particularly strong influence on O_3 formation (Weaver et al., 2009; Jacob and Winner, 2009), and the O_3–temperature relationship has been widely investigated. Vautard et al. (2005) and Pusede et al. (2015), for example, quantified the temperature sensitivity of ozone (ppb $°C^{-1}$) and reported an average sensitivity of 6.7 ± 2.5 ppb $°C^{-1}$ across major U.S. urban areas. Temperature-driven ozone increases have been attributed to faster oxidation chemistry involving NO_x and VOCs at higher temperatures (Atkinson, 2000). In addition, elevated temperatures enhance VOC emissions, particularly biogenic VOC (BVOC) emissions, thereby promoting additional O_3 production (Rasmussen et al., 2013). Bloomer et al. (2009) reported that O_3 concentrations increase under stagnant and extremely hot conditions such as heatwaves, and Pu et al. (2017) showed that strengthened stagnation and enhanced solar radiation during heatwaves in the Yangtze River Delta further intensified photochemical O_3 production.

However, most previous studies have focused on diagnostic analyses of historical temperature–O_3 relationships or individual heatwave cases. These studies have not been explicitly framed within the context of future regional climate change, particularly under IPCC climate scenarios. Moreover, biogeochemical feedbacks—such as temperature-driven changes in BVOC emissions—represent nonlinear and still uncertain processes in O_3 formation under a warming climate. Climate-driven changes in BVOC emissions may substantially modify O_3 production, especially in VOC-limited regimes, and may become more pronounced under future warming scenarios. Consequently, developing region-specific air quality policies that account for climate-induced temperature increases remains challenging, particularly given uncertainties in projecting regional climate change. In this study, we examine a historically observed extreme heat event as a physically plausible analog of near-future warming conditions, enabling assessment of urban air quality responses under elevated temperature scenarios.

South Korea provides a suitable setting for such an investigation. The country has experienced rapid warming and a marked increase in heatwave frequency over recent decades. The annual mean air temperature in South Korea has increased by approximately 0.9 °C over the past three decades (1990–2023), and the mean daily maximum temperature has increased by about 1 °C (KMA). According to the Ministry of Environment, the average summer heatwave frequency increased from 10.4 days during 1980–2000 to 31.5 days in 2018. Under the RCP4.5 scenario, heatwave risk in 2030 is projected to increase in approximately 26% of local municipalities relative to the 2000s (MOE, 2019), underscoring the growing relevance of heat-related air quality impacts.

At the same time, aggressive NO_x emission controls have been implemented in major metropolitan areas such as Seoul and Busan. South Korea has introduced a series of emission-reduction policies aimed at lowering anthropogenic NOx and VOC emissions, including the Special Act on Air Quality Improvement in Air Control Zones, seasonal PM management programs, strengthened vehicle-emission standards, and industrial VOC controls. These measures have contributed to long-term reductions in precursor emissions and improvements in air quality. However, despite these efforts, ozone concentrations have continued to increase in many urban areas, suggesting that climate-driven enhancement of photochemical ozone production may partially offset the benefits of anthropogenic emission-control strategies. Recent observations during the extreme 2018 heatwave in Seoul demonstrated that ozone formation accelerated with increasing temperatures, while fugitive anthropogenic VOC emissions and enhanced ozone production efficiency provided additional contributions to the observed ozone enhancement (Gil et al., 2026).

The response of ozone to emission reductions and climate-driven warming is strongly influenced by local chemical regimes and meteorological conditions. Because the response of ozone to warming depends strongly on the local chemical regime, it is important to distinguish between VOC-limited and NO_x-limited conditions. Previous studies have identified both Seoul and Busan as VOC-limited (or VOC-sensitive) ozone formation regimes based on satellite-derived formaldehyde-to-NO_2 ratios (FNRs) and supporting numerical analyses (Lee et al., 2021, 2022). This interpretation is also consistent with observation-based analyses conducted in the Seoul Metropolitan Area, which indicated VOC-sensitive ozone production and emphasized the importance of balanced NOx–VOC control strategies (Kim et al., 2020). Although Seoul and Busan differ in geography and local circulation—Busan being a coastal city and Seoul an inland megacity—both have experienced increasing heatwave risk, partly enhanced by urban heat-island effects that can further promote photochemical ozone formation (Zhao et al., 2019). These contrasting urban environments provide an opportunity to examine area-specific differences in O_3 responses to elevated temperature under comparable synoptic conditions.

Considering these contrasting geographic and meteorological characteristics, we use the extreme heatwave of summer 2018 as a realistic analog of elevated-temperature conditions to investigate how O_3 production responds to heat stress in two representative metropolitan environments. Specifically, we examine how temperature-dependent increases in BVOC emissions modify O_3 production sensitivity and discuss implications for attainable emission reduction strategies under a warming climate. This analysis is directly related to the concept of the climate change penalty for ozone, defined as the additional burden imposed on air quality management solely due to temperature increases induced by climate change. Our study aims to provide scientific insight into how climate-driven warming may influence ozone management in VOC-limited urban environments.

2. Data and methodology

2.1. Study areas, meteorological and air quality observations

Two metropolitan areas, Seoul and Busan, were selected as the study regions. Seoul represents a densely populated inland megacity, whereas Busan is a coastal urban area with relatively high annual mean O_3 concentrations. Previous studies have suggested that ozone formation mechanisms may differ between inland and coastal environments. Inland cities such as Seoul often experience stronger thermal accumulation, stagnant boundary-layer conditions, and prolonged photochemical processing, whereas Busan is additionally influenced by marine air masses and sea-breeze circulations that can modify pollutant dispersion and recirculation (Oh et al., 2006; Hwang et al., 2007; Kim et al., 2005). These contrasting meteorological characteristics provide a useful framework for examining regional differences in heatwave-associated ozone formation.

To characterize heatwave conditions and long-term heatwave occurrence, hourly observations of air temperature, wind speed, and precipitation were obtained from the Korea Meteorological Administration (KMA) Automated Synoptic Observing System (ASOS) in both metropolitan areas. The locations of the meteorological stations are shown in Fig. 1b and c. To examine long-term trends in heatwave occurrence, we additionally used annual heatwave-day statistics from the KMA Weather Data Service for the 51-year period from 1973 to 2023. Following the operational definition of the KMA, a heatwave day was identified when the daily maximum temperature was ≥33 °C.

For the analysis of ozone formation during heatwave and non-heatwave conditions, air quality data and advisory records were obtained from AirKorea, the National Ambient Air Quality Monitoring Network operated by the Ministry of Environment (MOE) and the Korea

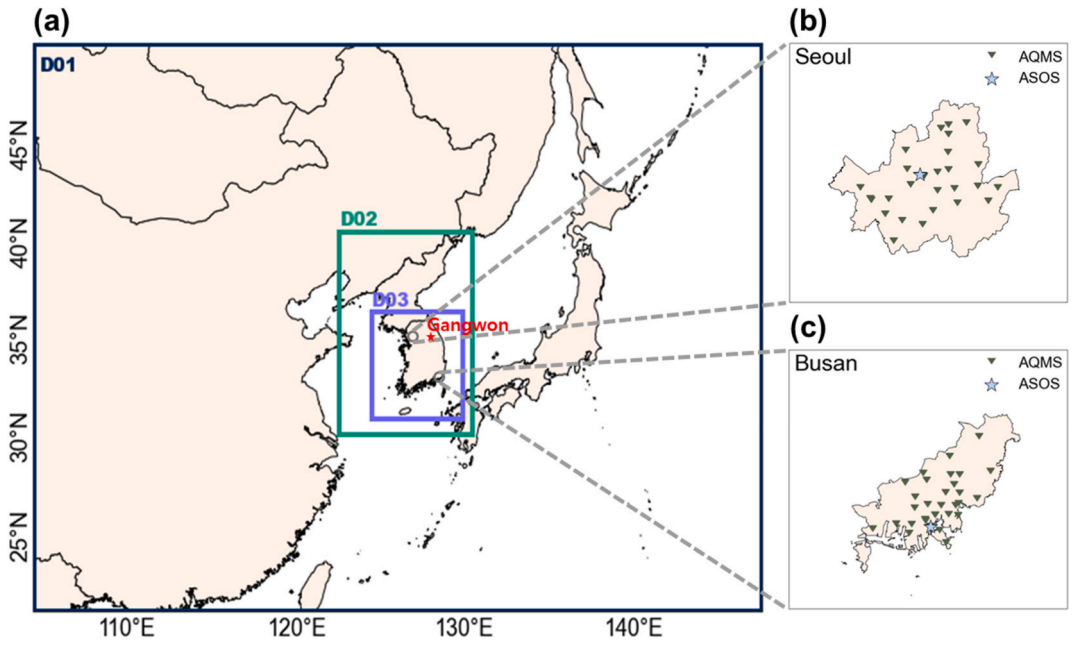

Fig. 1. Model domains and observation sites used in this study. The outer, intermediate, and inner domains (D01-D03) are shown in the left panel. The right panels show the distributions of air quality monitoring stations (AQMS; triangles) and an automated surface observing system site (ASOS; star) within Seoul and Busan.

Environment Corporation (KECO). Hourly O_3 and NO_2 concentrations from 27 monitoring sites in Seoul and 28 sites in Busan were used in this study (Fig. 1). To characterize long-term high-ozone occurrence, we also analyzed O_3 advisory records from AirKorea for the period 1995–2023. A high-O_3 day was defined as a day on which the 1-h mean ozone concentration reached or exceeded 120 ppb, corresponding to the official AirKorea ozone advisory criterion.

2.2. WRF-Chem model configuration

We employed the online-coupled WRF-Chem (Weather Research and Forecasting–Chemistry) model (version 3.9.1), which integrates atmospheric chemistry within the WRF framework to simulate atmospheric dynamics and mesoscale physical processes, including cloud microphysics. Topographic data and meteorological initial and lateral boundary conditions were generated using the WRF Preprocessing System (WPS). Time integration was conducted using the Advanced Research WRF (ARW) dynamical core to produce three-dimensional meteorological and chemical fields (Grell et al., 2005).

Three one-way nested domains were configured with horizontal grid spacings of 27 km (D01), 9 km (D02), and 3 km (D03), as shown in Fig. 1a. The simulation period, including spin-up, covered the prolonged heatwave episode from 00:00 UTC 27 June 2018 to 00:00 UTC 1 September 2018. Meteorological initial and boundary conditions were provided by the National Centers for Environmental Prediction (NCEP) Final Operational Global Analysis (FNL). Detailed physical and chemical parameterizations used in the WRF-Chem simulations are summarized in Table S1.

Anthropogenic emissions were based on the KORUSv5 inventory, which was developed using the bottom-up CREATE emission inventory framework for Asia as a foundation (Woo et al., 2020). The emissions were processed through the SMOKE-Asia framework (Woo et al., 2012). No additional heatwave-specific or temperature-dependent scaling was applied to anthropogenic VOC emissions during the simulation period. Therefore, anthropogenic VOC emissions followed the prescribed temporal profiles of the inventory throughout the simulation.

In contrast, BVOC emissions were calculated online using MEGAN version 2.04 (Model of Emissions of Gases and Aerosols from Nature) as a function of meteorological variables, including temperature and solar radiation. This configuration allows heatwave-related changes in ozone formation to be interpreted primarily in terms of meteorology-dependent BVOC emissions under a fixed anthropogenic emission framework.

2.3. TROPOMI satellite data

To characterize VOC-related variability, particularly formaldehyde (HCHO) as a key oxidation product of BVOCs, we used satellite retrievals from the TROPOspheric Monitoring Instrument (TROPOMI) onboard Sentinel-5 Precursor (Sentinel-5P). TROPOMI is a nadir-viewing imaging spectrometer operating in the ultraviolet, visible, near-infrared, and shortwave infrared spectral ranges, providing near-global daily coverage with a swath width of approximately 2600 km. During the study period, the typical nadir pixel size was approximately $7 \times 3.5\ km^2$, and the satellite provided one daytime observation per location in the early afternoon, with an ascending-node equator-crossing time of about 13:30 local solar time.

TROPOMI provides Level-2 atmospheric composition products, including O_3, NO_2, HCHO, SO_2, CH_4, CO, and aerosol-related variables. In this study, we used the Level-2 HCHO product to investigate the spatial and temporal variability of HCHO over the study region. For quality control, only pixels with a quality assurance value (qa_value) ≥ 0.8 were retained, and scenes with a cloud fraction ≥ 0.4 were excluded. This criterion is more conservative than the recommended threshold (qa_value > 0.5) to reduce cloud-related retrieval uncertainty (De Smedt et al., 2023). After quality control, the TROPOMI L2 HCHO pixels were interpolated onto a regular latitude–longitude grid using linear interpolation to visualize broad spatial patterns.

The native TROPOMI HCHO footprint (approximately $7 \times 3.5\ km^2$) is larger than the 3-km horizontal grid spacing of the innermost WRF-Chem domain. Therefore, the satellite retrievals were not remapped directly onto the WRF-Chem grid, because such remapping would oversample the satellite product beyond its native footprint and could introduce artificial fine-scale spatial structures, particularly after cloud and quality filtering have reduced the number of valid pixels. Accordingly, TROPOMI HCHO was not used for strict grid-to-grid validation of modeled HCHO concentrations. Instead, it was used to evaluate broad spatial patterns and relative heatwave-related enhancements. Therefore,

satellite–model comparisons presented in this study should be interpreted in terms of pattern-level consistency rather than exact quantitative agreement.

Previous validation studies have reported a retrieval uncertainty of approximately 31% relative to selected ground-based observations (De Smedt et al., 2023). Therefore, TROPOMI HCHO is used in this study primarily as an indicator of BVOC-related oxidation and relative enhancement rather than as a direct quantitative constraint on BVOC emissions.

3. Results

3.1. Trends in heatwave and high-ozone episodes

Fig. 2 presents the time series of heatwave occurrence in the two study areas. In Seoul, except for 1994 as an anomalously high year, the annual number of heatwave days remained within a relatively constrained range prior to 2010, with pronounced interannual variability (Fig. 2a). Since 2010, however, the upper envelope of heatwave occurrence has increased steadily, indicating an intensification of extreme heat events. Busan shows a broadly similar pattern: before 2012, annual heatwave days rarely exceeded 10 and exhibited strong year-to-year variability, whereas a gradual upward trend is evident thereafter. The year 2018 stands out as the most extreme year in both cities, with 35 heatwave days in Seoul and 18 in Busan (Fig. 2b).

This tendency is also reflected in the seasonal distribution of heatwaves based on cumulative monthly counts (Fig. 3). Comparing the recent 26-year period (1998–2023) with the earlier 25-year period (1973–1997), Seoul experienced substantial increases in summer heatwaves, with increases of 55.6% in June, 43.3% in July, and 53.3% in August. Busan exhibited a more complex pattern, with no heatwave occurrence in June, a 33.3% decrease in July, and a 150% increase in August. As a coastal city, Busan is subject to strong maritime modulation, which can produce more variable heatwave responses (Zhou et al., 2019; Wie et al., 2021). Nevertheless, the overall comparison indicates that heatwave occurrence has increased substantially in recent decades, consistent with expectations under a warming climate.

An increasing tendency in high-ozone episodes is also evident in both areas. Fig. 4 shows the time series of O_3 advisory occurrences; a national O_3 advisory is issued when the 1-h mean concentration reaches or exceeds 120 ppb. In Seoul, annual advisories generally remained below 20 prior to 2016 but exceeded 30 thereafter, reaching 54 in 2018 (Fig. 4a). Busan exhibited a similar shift, with advisories generally at or below 10 per year prior to 2012, followed by a sustained increase and reaching 24 in 2018 (Fig. 4b). Taken together, the concurrent increases in heatwave occurrence and high-O_3 advisories suggest strong co-variability between extreme heat and ozone pollution, consistent with enhanced photochemical production and stagnation-favorable meteorological conditions during heatwave periods.

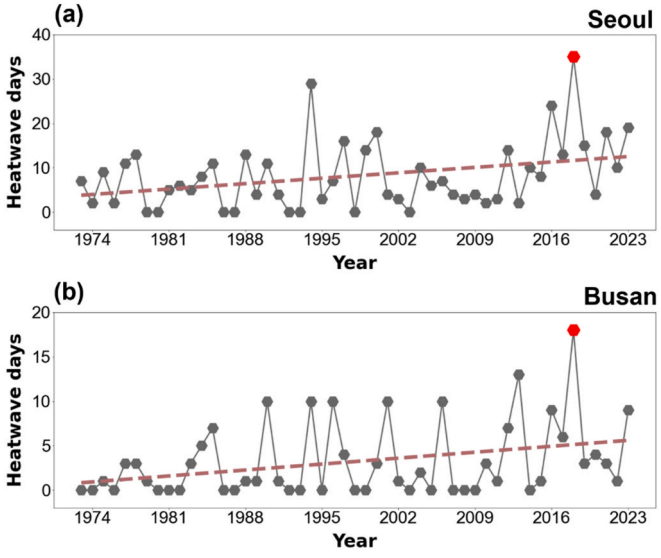

Fig. 2. Interannual variation in annual heatwave days during 1973-2023 for (a) Seoul and (b) Busan. Gray markers indicate annual values, the dashed line denotes the linear trend, and the red marker highlights the year with the maximum number of heatwave days.

3.2. Model evaluation

The performance of WRF-Chem was evaluated for the summer of 2018. Simulated 2-m air temperature, 10-m wind speed, relative humidity, and surface ozone were compared with ASOS and AirKorea observations for both Seoul and Busan (Fig. S1). Model performance was assessed using the correlation coefficient (R) and the index of agreement (IOA).

Temperature, the key variable for identifying heatwave days, showed good agreement with observations (Seoul: R = 0.92, IOA = 0.95; Busan: R = 0.91, IOA = 0.95). Wind speed showed lower performance (Seoul: R = 0.45, IOA = 0.48; Busan: R = 0.49, IOA = 0.64), whereas relative humidity was reasonably reproduced in both cities (Seoul: R = 0.81, IOA = 0.88; Busan: R = 0.70, IOA = 0.82). The relatively lower performance for wind speed is consistent with previous mesoscale-model evaluation studies, which have shown that wind fields are generally more difficult to reproduce because they are strongly influenced by local topography, surface roughness, and boundary-layer processes (Emery et al., 2017). Although uncertainty in simulated wind fields may affect pollutant transport, ventilation, and boundary-layer mixing, the model performance remained within commonly accepted evaluation ranges for regional meteorological simulations.

For ozone, R was 0.80 in Seoul and 0.73 in Busan, with IOA values of 0.85 at both sites, indicating that the model reasonably reproduced observed ozone variability. Because precipitation can influence ozone and precursor concentrations through wet scavenging, subsequent analyses focused on the period from 6 July to 20 August 2018, thereby minimizing precipitation-related interference and isolating heatwave-associated ozone enhancement processes.

3.3. Chemical variations of O_3, HCHO, and NO_2

Fig. 5 shows WRF-Chem simulated O_3, HCHO, and NO_2 concentrations during 6 July–20 August 2018. In Seoul, elevated temperatures coincided well with high ozone days, particularly during identified heatwave events. In Seoul, the mean air temperature during periods when O_3 exceeded 80 ppb was 37.7 °C. HCHO increased largely in phase with the high-O_3 period, with a mean concentration of approximately 9 ppb, which is about 5.5 ppb higher than the study-period average. In contrast, NO_2 concentrations did not show a clear temperature-dependent pattern and were not closely aligned with elevated O_3 levels.

In Busan, the linkage between high temperature and high O_3 was somewhat less pronounced than in Seoul; however, high-ozone events still tended to occur on warmer days. Only one instance exceeded 80 ppb, and the air temperature during that period was 32.1 °C. The mean temperature for hours with O_3 above 70 ppb was 32.2 °C. HCHO also increased during the high-ozone period, with a mean concentration of 4.6 ppb, approximately 2.5 ppb higher than the study-period average.

Overall, both areas exhibited enhanced O_3 under high-temperature conditions relative to typical days, with HCHO showing a consistent tendency. The correlation between O_3 and HCHO was 0.67 in Seoul, whereas the correlation between O_3 and NO_2 was −0.14. In Busan, the O_3–HCHO correlation was 0.39, compared with −0.52 for O_3–NO_2. These results indicate that HCHO is more strongly associated with O_3 variability than NO_2 during high-ozone conditions, although regional

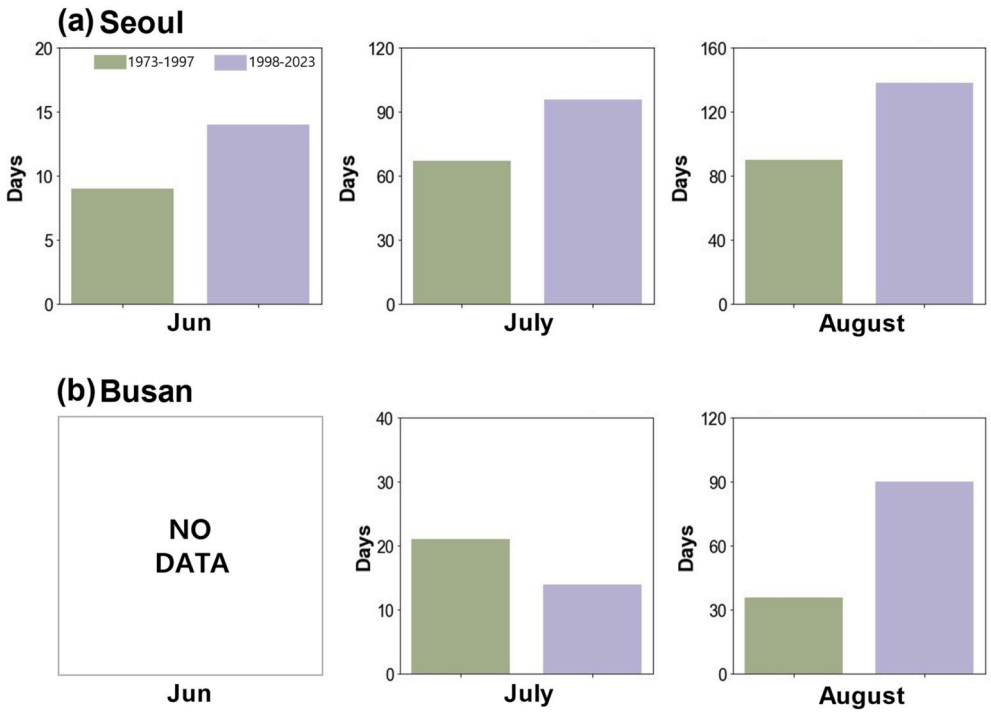

Fig. 3. Cumulative monthly heatwave days for June, July, and August accumulated over two periods (1973–1997 and 1998–2023) in (a) Seoul and (b) Busan. Green and purple bars indicate the total number of heatwave days accumulated within each month over 1973–1997 and 1998–2023, respectively. "NO DATA" denotes unavailable records for the corresponding month/period.

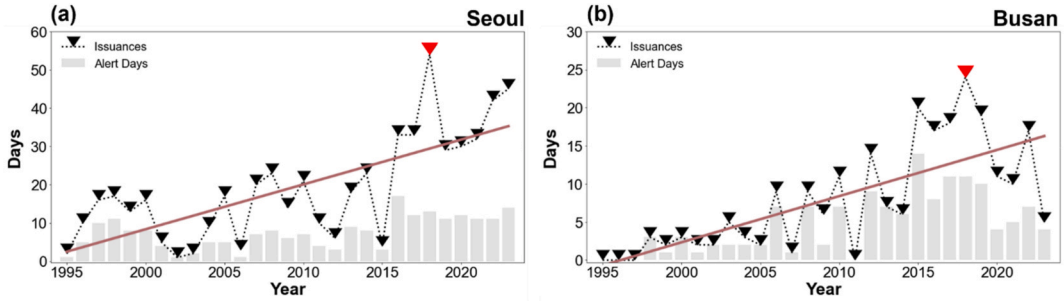

Fig. 4. Interannual variations in ozone advisory issuances and advisory days during 1995–2023 for (a) Seoul and (b) Busan. Gray bars indicate the number of ozone advisory days, and black triangles connected by a dotted line denote the annual number of issuances. Solid lines represent linear trends, and red markers highlight the year with the maximum number of issuances.

differences likely reflect local geographic and meteorological influences.

Fig. 6 compares diurnal variations of T2, O_3, HCHO, and NO_2 between heatwave and non-heatwave days in Seoul, Busan, and a forested site in Gangwon Province (denoted in Fig. 1), located east of Seoul. In Seoul, heatwave days showed a clear thermal contrast relative to non-heatwave days, with the composite maximum and mean T2 increasing by 5.5 °C and 5.0 °C, respectively. Under these warmer conditions, mean O_3 concentrations were 18.2 ppb on heatwave days and 12.4 ppb on non-heatwave days, with peak values of 48.50 ppb and 25.47 ppb, respectively. HCHO also increased during heatwaves, with mean concentrations rising from 2.4 to 3.7 ppb and peak concentrations increasing by approximately 2.9 ppb. In contrast, NO_2 showed only minor differences between the two categories.

Busan exhibited a similar tendency. The composite maximum and mean T2 increased by 3.8 °C and 2.6 °C, respectively. Mean O_3 concentrations were 29.12 ppb and 26.89 ppb on heatwave and non-heatwave days, respectively, with peak O_3 approximately 16 ppb higher during heatwave days. HCHO also increased during heatwaves, with the mean concentration higher by 0.9 ppb relative to non-heatwave days, and the peak concentration higher by 2.2 ppb. For NO_2, as in Seoul, differences between heatwave and non-heatwave conditions were minimal.

The Gangwon site, characterized by high HCHO and relatively low NO_2, represents a NO_x-limited regime. This site showed a pronounced heatwave-related temperature increase, with the composite maximum and mean T2 increasing by 6.7 °C and 4.6 °C, respectively. Here, mean O_3 concentrations increased by approximately 10 ppb during heatwave days, and peak O_3 differences reached 24 ppb—the largest among the three regions. HCHO showed a strong heatwave-related increase, while NO_2 remained substantially lower than in the urban areas. These results indicate that elevated temperatures were consistently accompanied by enhanced HCHO and O_3 concentrations, supporting a close linkage between heat stress, BVOC-related oxidation, and photochemical ozone production.

The statistical distributions of key meteorological variables—temperature, wind speed, and relative humidity—during heatwave and non-heatwave days are shown in Fig. S2 for three regions: Seoul, Busan, and Gangwon Province. In all regions, heatwave

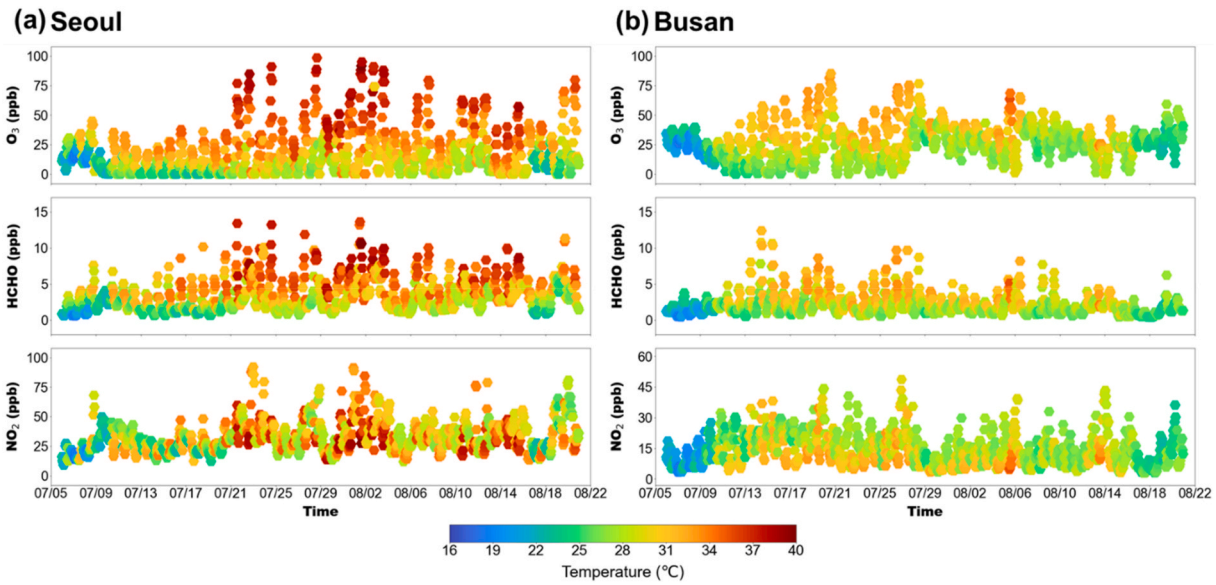

Fig. 5. Temperature dependence of simulated pollutant concentrations in 6 July-20 August 2018 for (a) Seoul (left) and (b) Busan (right). Hourly modeled O_3, HCHO, and NO_2 concentrations are shown as scatter points, with marker color indicating air temperature (°C).

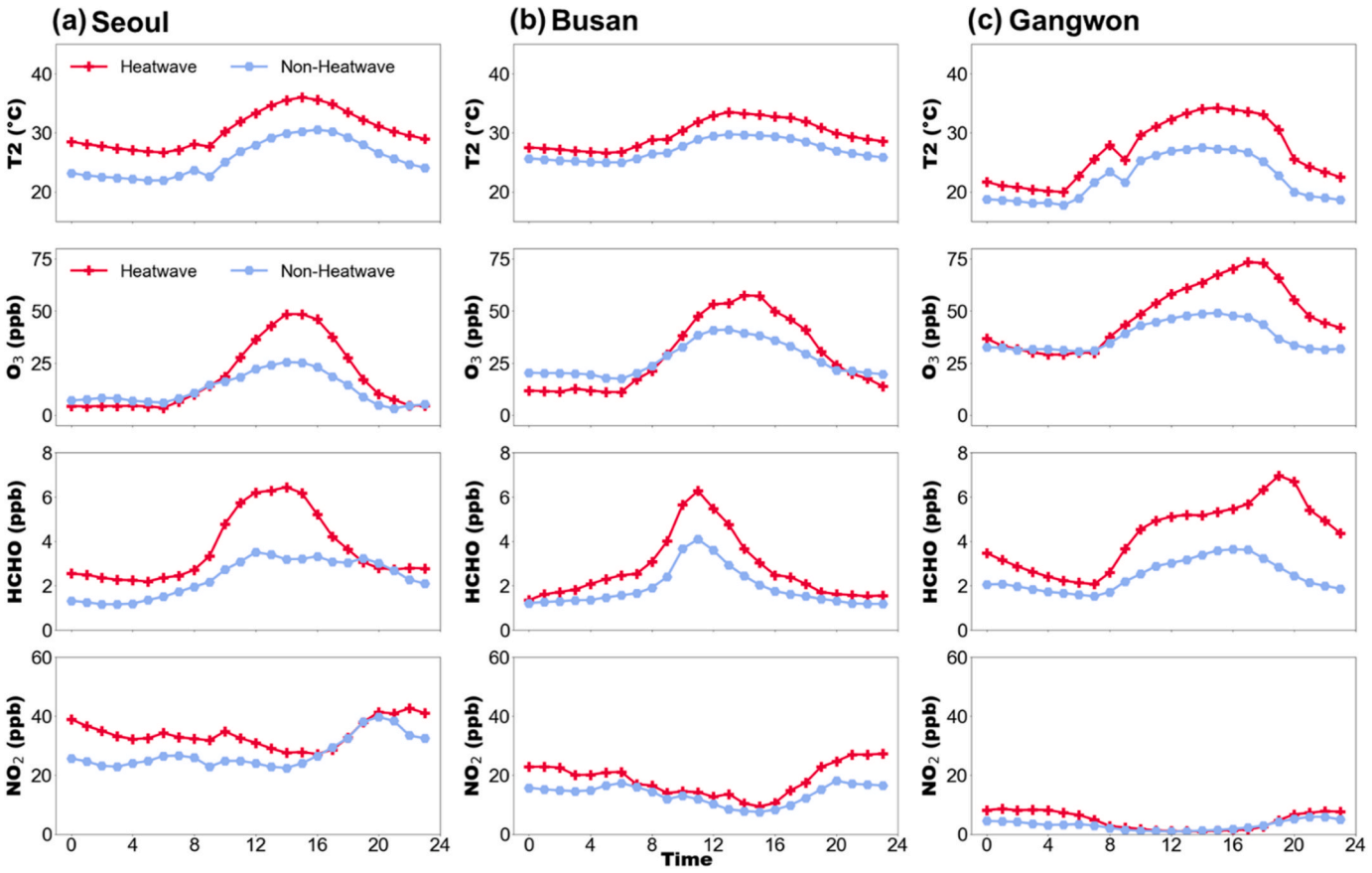

Fig. 6. Diurnal variations of 2-m air temperature (T2), O_3, HCHO and NO_2 under heatwave and non-heatwave conditions for (a) Seoul, (b) Busan, and (c) Gangwon Province. Red and blue lines denote mean diurnal cycles for heatwave and non-heatwave days, respectively. Time is local standard time (0–23 h). Temperature is in °C, and chemical concentrations are in ppb.

conditions were characterized by higher temperatures, reduced wind speeds, and lower relative humidity, creating meteorological conditions favorable for ozone accumulation and photochemical production.

3.4. *Ozone and its association with temperature, HCHO, and BVOC*

To further examine differences in HCHO distributions between heatwave and non-heatwave days, WRF-Chem simulations (Fig. 7a and

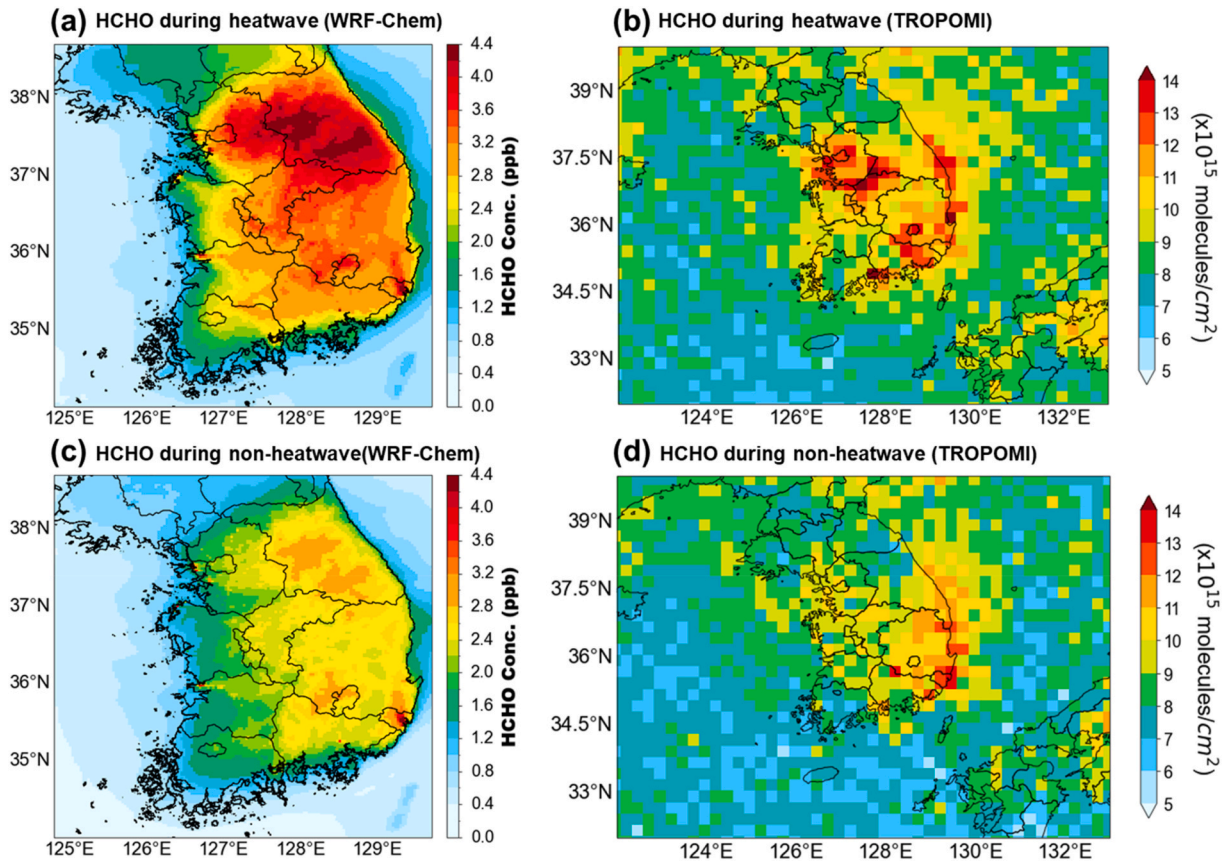

Fig. 7. Spatial distributions of HCHO during heatwave (top) and non-heatwave (bottom) days. The left panels show simulated surface HCHO concentrations (ppb), and the right panels show TROPOMI HCHO vertical column densities ($\times 10^{15}$ molecules cm^{-2}). Both fields are averaged over 6 July-20 August 2018.

c) and TROPOMI observations (Fig. 7b and d) were analyzed. The model results show elevated HCHO during heatwave conditions, particularly over the forested Gangwon region, where concentrations exceeded 4 ppb. Enhanced HCHO was also evident over Seoul, while Busan showed relatively lower levels. During non-heatwave periods, HCHO concentrations generally remained between 1 and 2 ppb. TROPOMI observations showed a similar spatial tendency. Although the satellite provides only one daytime observation per day, the mean HCHO concentration during heatwave periods was consistently higher than during non-heatwave periods, supporting the modeled results.

Fig. 8 presents scatter plots of temperature versus HCHO and O_3 from WRF-Chem simulations for Seoul and Busan. The fitted curves indicate a nonlinear relationship with a quadratic (second-order) tendency. Using daily maximum concentrations, temperature showed a strong positive association with HCHO ($R = 0.59$) and O_3 ($R = 0.69$) in Seoul. In Busan, the corresponding correlations were $R = 0.60$ (HCHO) and $R = 0.57$ (O_3). The relatively weaker relationship in Busan likely reflects the narrower temperature range during the study period, with maximum temperatures approximately 5 °C lower than in Seoul. In addition, Busan's coastal setting may have contributed to the weaker and more variable response. Maritime influences and land–sea-breeze circulations can affect local ventilation, pollutant transport, and precursor recirculation, and previous studies have shown that sea-breeze evolution can influence O_3 distributions over the Busan metropolitan area (Oh et al., 2006). Although a dedicated sea-breeze classification was not conducted in this study, coastal meteorological modulation likely contributes to the different O_3–temperature relationship observed between Busan and inland Seoul.

4. Discussion

O_3 is produced through complex formation and destruction pathways involving its key precursors, nitrogen oxides (NO_x) and volatile organic compounds (VOCs). Among the controlling factors, temperature plays a critical role in regulating both precursor abundances and photochemical reaction rates. Quantitative evaluation of temperature-dependent photochemical processes can be achieved through analytical interpretation of reaction kinetics or sensitivity experiments using chemical transport or box models.

Most previous studies have implicitly assumed that precursor emissions remain constant with increasing temperature. However, certain VOC species—particularly biogenic VOCs (BVOCs)—are highly temperature sensitive. Elevated temperatures enhance BVOC emissions, increasing their participation in atmospheric photochemical reactions (Kleist et al., 2012). However, the magnitude of this temperature response can vary depending on vegetation type, land-cover distribution, light availability, soil moisture, heat or drought stress, and the BVOC emission parameterization used in the model (Peñuelas and Staudt, 2010; Guenther et al., 2012). Enhanced BVOC oxidation promotes the production of reactive radicals, contributing to increased HCHO formation and subsequently enhanced ozone production. Consequently, during heatwave periods characterized by high temperatures, BVOC emissions can increase substantially. Although BVOC concentrations cannot be directly retrieved from satellite observations, HCHO distributions can be observed and used as a proxy for BVOC oxidation.

Among BVOCs, isoprene plays a particularly important role in intensifying NO_x–O_3 photochemical cycling (Calfapietra et al., 2009). Approximately 67% of more than 1800 investigated plant species are reported to emit isoprene, and nearly 70% of total isoprene emissions

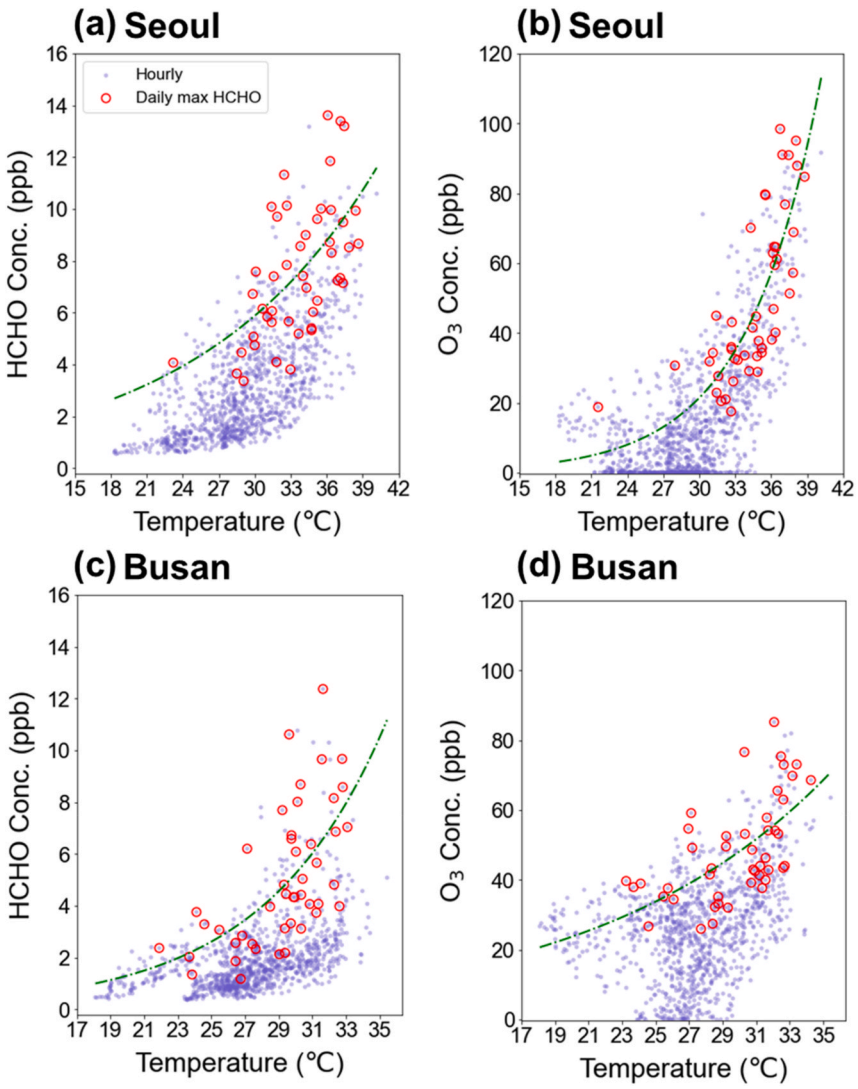

Fig. 8. Relationships between air temperature and (a, c) HCHO and (b, d) O_3 in 6 July-20 August 2018 for Seoul (a–b) and Busan (c–d). Purple dots show hourly values, and red circles indicate daily maximum concentrations. Green dashed lines represent fitted curves illustrating the temperature dependence of HCHO and O_3.

originate from deciduous broadleaf forests (Wiedinmyer et al., 2004; Laothawornkitkul et al., 2009). The simplified oxidation pathway contributing to ozone formation can be expressed as:

$$\text{Isoprene} + \text{OH} \rightarrow \text{RO}_2 \quad \text{(R1)}$$

$$\text{RO}_2 + \text{NO} \rightarrow \text{RO} + \text{NO}_2 \quad \text{(R2)}$$

$$\text{RO} + \text{O}_2 \rightarrow \text{HCHO} + \text{HO}_2 \quad \text{(R3)}$$

$$\text{HO}_2 + \text{NO} \rightarrow \text{NO}_2 + \text{OH} \quad \text{(R4)}$$

$$\text{NO}_2 + \text{h}\nu \rightarrow \text{O} + \text{NO} \quad \text{(R5)}$$

$$\text{O} + \text{O}_2 \rightarrow \text{O}_3 \quad \text{(R6)}$$

Isoprene reacts rapidly in the atmosphere via reaction (R1), typically within approximately 1 h (Wells et al., 2020). During its oxidation, organic peroxy radicals (RO_2) are formed, which subsequently produce formaldehyde (HCHO) through reactions (R2) and (R3), and eventually contribute to ozone formation through reactions (R4–R6). Because the atmospheric lifetime of HCHO is longer than that of isoprene (Palmer et al., 2003) and HCHO can be observed from satellite platforms, it is commonly used as a tracer for isoprene-related BVOC oxidation.

The forest distribution over South Korea, derived from MODIS data (Fig. S3), indicates that deciduous broadleaf forests account for approximately 59.6% of total forested area, with mixed forests representing 27.8%. These forests are primarily concentrated in the Gangwon region, the extensive forested area east of Seoul. In this study, HCHO distributions were analyzed using TROPOMI retrievals, while BVOC dynamics were examined using WRF-Chem simulations. The spatial correspondence between elevated HCHO and forested regions suggests that observed HCHO enhancements are closely linked to temperature-driven BVOC emissions. Taken together, satellite observations and model simulations indicate that enhanced BVOC emissions from forested areas contribute to elevated O_3 during heatwave periods. Although this study focuses on South Korean megacities, similar heatwave-related O_3 enhancement has been reported in other urban and industrialized regions, including Europe during the 2003 heatwave (Vautard et al., 2005), the Yangtze River Delta during the 2013 heatwave (Pu et al., 2017), and the New York City metropolitan region (Zhao et al., 2019). Therefore, the heatwave-enhanced BVOC/HCHO–O_3 mechanism discussed here may also be relevant to other VOC-sensitive urban or industrial regions where sufficient NO_x, strong solar radiation, and nearby biogenic emission sources coexist. However, the magnitude of this response is expected to vary depending on local NO_x–VOC sensitivity, vegetation type, land-cover distribution, background O_3, and meteorological conditions.

To further evaluate the role of BVOC emissions, an additional

sensitivity simulation was conducted with the MEGAN biogenic emission module disabled (No-MEGAN experiment; Fig. 9). Relative to the baseline simulation, the exclusion of BVOC emissions reduced the daily maximum O_3 concentration in Seoul from 50.5 to 34.2 ppb (−32.3%) and HCHO from 6.6 to 3.9 ppb (−40.9%). Similar but slightly weaker responses were observed in Busan, where O_3 and HCHO decreased by 25.9% and 40.0%, respectively. The reductions were most pronounced during daytime when photochemical activity was strongest, whereas nighttime differences were relatively small. These results provide direct model-based evidence that temperature-enhanced BVOC emissions substantially contribute to HCHO formation and ozone enhancement during heatwave conditions.

Although elevated temperature is generally recognized as a major driver of BVOC emissions, uncertainties remain in the quantitative estimation of BVOC emissions because MEGAN-derived emissions depend on vegetation distribution and emission parameterizations (Guenther et al., 2012). Therefore, HCHO should be interpreted as supporting evidence of BVOC-related oxidation rather than as a direct quantitative estimate of BVOC emissions. Nevertheless, the sensitivity experiment (Fig. 9), together with the observed increases in temperature, HCHO, and ozone, supports the conclusion that BVOC emissions contribute substantially to ozone enhancement during heatwave conditions. Similar to other environmental systems that exhibit amplified responses to warming (Wu et al., 2025), our results suggest that elevated temperatures can induce nonlinear changes in atmospheric chemical processes through enhanced BVOC emissions and ozone production, implying that BVOC–HCHO–O_3 chemistry may be further amplified under continued climate warming.

This mechanism is directly related to the concept of the climate change penalty for ozone, defined as the additional burden on air quality management arising solely from climate-induced temperature increases, independent of anthropogenic emission trends. Our findings suggest that climate-driven enhancements in ozone formation should be explicitly considered when designing and evaluating emission control strategies under future warming scenarios. In the present study, anthropogenic VOC emissions were prescribed and were not additionally scaled with temperature, whereas BVOC emissions responded dynamically to meteorological conditions through MEGAN. Together with the BVOC sensitivity experiment (Fig. 9), this framework enables the evaluation of a temperature-sensitive photochemical pathway under a given anthropogenic emission environment. Although this does not provide a complete quantitative separation of climate and emission effects, it provides direct evidence that temperature-responsive BVOC emissions can substantially enhance ozone formation during heatwave conditions.

One limitation of this study is that the analysis is based on a single historical heatwave event (summer 2018), which cannot fully represent the complexity of future climate change. Therefore, the present study should not be interpreted as a deterministic projection of future ozone levels under specific climate scenarios. Instead, the 2018 heatwave is used as an observational analog of physically plausible high-temperature conditions that may become more frequent under continued climate warming. Despite this limitation, the observed

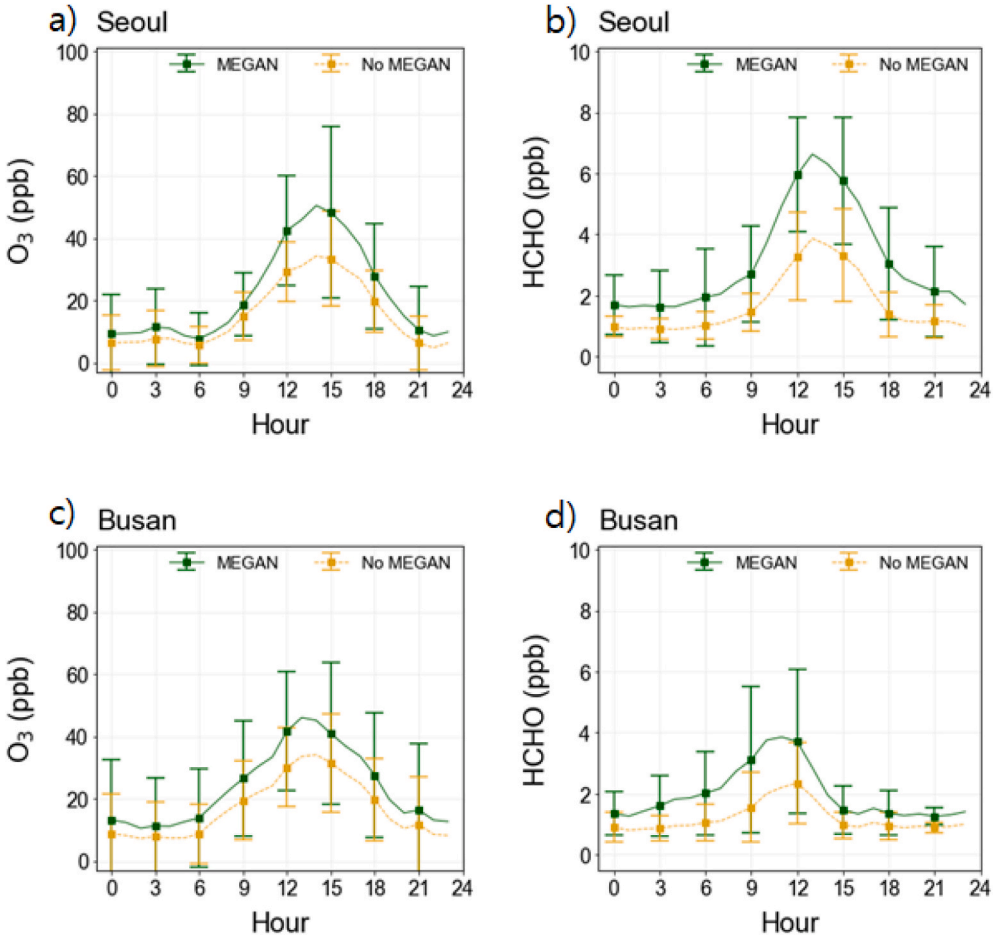

Fig. 9. Diurnal variations of simulated O_3 and HCHO concentrations in Seoul and Busan during the study period (27 June 2018–1 September 2018) from WRF-Chem simulations with the biogenic VOC (BVOC) emission module MEGAN turned on (MEGAN) and off (No-MEGAN): (a) O_3 in Seoul, (b) HCHO in Seoul, (c) O_3 in Busan, and (d) HCHO in Busan. The differences between the two simulations represent the contribution of BVOC emissions to HCHO formation and O_3 enhancement. Error bars indicate ±1 standard deviation.

relationships among temperature, HCHO, and ozone provide useful insight into the mechanisms through which future warming may influence ozone formation in VOC-limited urban environments.

5. Summary and conclusions

Although primary emissions and photochemical processes are fundamental to O_3 production, climate-related warming associated with extreme heat events also plays an important role in modulating ozone levels. To characterize O_3 formation under climate-induced temperature increases, we analyzed meteorological observations from ASOS and air quality data from two metropolitan areas in South Korea. The unprecedented heatwave during the summer of 2018 was examined as a physically plausible analog of near-future warming conditions, and chemical characteristics during heatwave days were compared with those during non-heatwave days. In addition, we investigated variations in O_3, BVOC-related HCHO, and associated temperature dependence using satellite observations and WRF-Chem simulations.

Our results demonstrate a clear association between temperature and O_3. Satellite observations showed that HCHO enhancements were substantially greater during heatwave days than during non-heatwave periods. The concurrent occurrence of elevated HCHO and high O_3 indicates that temperature-driven BVOC oxidation contributes to enhanced ozone formation under high-temperature conditions. WRF-Chem simulations further support this interpretation by linking increased HCHO during heatwave episodes to temperature-dependent BVOC emissions. Together, these findings highlight the importance of the BVOC–HCHO–O_3 chain in the context of climate-driven ozone enhancement.

These results have important implications for air quality management. The temperature-driven amplification of ozone formation represents a potential climate change penalty, whereby warming alone can partially offset the benefits of anthropogenic emission reductions. Heatwave-enhanced photochemistry and temperature-dependent BVOC emissions may therefore impose an additional burden on ozone management under existing anthropogenic precursor-control efforts. Similar mechanisms may also operate in other VOC-sensitive urban and industrial regions where elevated temperatures, abundant NO_x, and nearby biogenic emission sources coexist, although the magnitude of the response is likely to vary depending on local chemical sensitivity and meteorological conditions. Therefore, rigorous assessment of the climate–ozone linkage is essential for developing effective and achievable air quality management strategies under future warming scenarios. Accounting for the warming-driven tendency toward ozone enhancement under climate change will be critical in designing robust mitigation policies for VOC-limited urban environments, as substantially greater reductions in precursor emissions may be required to offset the climate-driven increase in ozone under continued warming.

CRediT authorship contribution statement

Han-Jun Ji: Conceptualization, Data curation, Writing – original draft. **Hyo-Jung Lee:** Conceptualization, Supervision, Validation. **Jong-Min Kim:** Software, Validation. **Sang-Seok Oh:** Validation, Visualization. **Min-Seong Kim:** Validation, Visualization. **Cheol-Hee Kim:** Conceptualization, Supervision, Writing – review & editing.

Declaration of competing interest

The authors declare that they have no known competing financial interests or personal relationships that could have appeared to influence the work reported in this paper.

Acknowledgement

This work was supported by the Basic Science Research Program through the National Research Foundation of Korea (NRF), funded by the Ministry of Education (RS-2020-NR049592) and (RS-2020-NR054792).

Appendix A. Supplementary data

Supplementary data to this article can be found online at https://doi.org/10.1016/j.jenvman.2026.130358.

Data availability

Data will be made available on request.

References

Atkinson, R., 2000. Atmospheric chemistry of VOCs and NOx. Atmos. Environ. 34 (12–14), 2063–2101. https://doi.org/10.1016/S1352-2310(99)00460-4.

Bloomer, B.J., Stehr, J.W., Piety, C.A., Salawitch, R.J., Dickerson, R.R., 2009. Observed relationships of ozone air pollution with temperature and emissions. Geophys. Res. Lett. 36 (9), L09803. https://doi.org/10.1029/2009GL037308.

Calfapietra, C., Fares, S., Loreto, F., 2009. Volatile organic compounds from Italian vegetation and their interaction with ozone. Environ. Pollut. 157 (5), 1478–1486. https://doi.org/10.1016/j.envpol.2008.09.048.

Colombi, N.K., Jacob, D.J., Yang, L.H., Zhai, S., Shah, V., Grange, S.K., Yantosca, R.M., Kim, S., Liao, H., 2023. Why is ozone in South Korea and the Seoul metropolitan area so high and increasing? Atmos. Chem. Phys. 23 (7), 4031–4044. https://doi.org/10.5194/acp-23-4031-2023.

De Smedt, I., Romahn, F., Eichmann, K.-U., 2023. S5P Mission Performance Centre Formaldehyde [L2_HCHO__] Readme. European Space Agency, Issue 2.6. https://sentinels.copernicus.eu/documents/247904/3541451/Sentinel-5P-Formaldehyde-Readme.pdf.

Ding, S., Cao, S., Sun, Y., Zhao, S., Xu, B., Liu, D., 2025. Health burden and associated economic losses attributable to atmospheric Black carbon in Hangzhou, East China: characteristics, source apportionment and policy implications. Atmos. Environ. 363, 121615. https://doi.org/10.1016/j.atmosenv.2025.121615.

Emery, Christopher, Liu, Zhen, Russell, Armistead G., Odman, M. Talat, Yarwood, Greg, Kumar, Naresh, 2017. Recommendations on statistics and benchmarks to assess photochemical model performance. Journal of the Air & Waste Management Association 67 (5), 582–598. https://doi.org/10.1080/10962247.2016.1265027.

Gil, J., Lee, M., Park, M., Kim, C.-H., Koo, J., Lee, H., Kang, S., Rhee, H., 2026. Accelerated O_3 formation triggered by summer heatwaves in megacity Seoul. Environ. Sci. Process. Impacts 28 (3), 752–762. https://doi.org/10.1039/D5EM00629E.

Grell, G.A., Peckham, S.E., Schmitz, R., McKeen, S.A., Frost, G., Skamarock, W.C., Eder, B., 2005. Fully coupled "online" chemistry within the WRF model. Atmos. Environ. 39 (37), 6957–6975. https://doi.org/10.1016/j.atmosenv.2005.04.027.

Guenther, A.B., Jiang, X., Heald, C.L., Sakulyanontvittaya, T., Duhl, T., Emmons, L.K., Wang, X., 2012. The model of emissions of gases and aerosols from nature version 2.1 (MEGAN2.1): an extended and updated framework for modeling biogenic emissions. Geosci. Model Dev. 5 (6), 1471–1492. https://doi.org/10.5194/gmd-5-1471-2012.

Hwang, M.-K., Kim, Y.-K., Oh, I.-B., Lee, H.W., Kim, C.-H., 2007. Identification and interpretation of representative ozone distributions in association with the sea breeze from different synoptic winds over the coastal urban area in Korea. J. Air Waste Manag. Assoc. 57 (12), 1480–1488. https://doi.org/10.3155/1047-3289.57.12.1480.

Intergovernmental Panel on Climate Change, 2021. Climate Change 2021: the Physical Science Basis. Cambridge University Press. https://doi.org/10.1017/9781009157896.

Jacob, D.J., Winner, D.A., 2009. Effect of climate change on air quality. Atmos. Environ. 43 (1), 51–63. https://doi.org/10.1016/j.atmosenv.2008.09.051.

Jin, H., Yeo, S., Woo, J.-H., Kim, M.J., Seong, M., Seo, D.H., Baek, J., Oh, S.-S., Kim, C.-H., 2025. Impact of the 2050 carbon-neutral emission scenario on air quality in South Korea. J. Environ. Manag. 385, 125653. https://doi.org/10.1016/j.jenvman.2025.125653.

Kim, C.-H., Park, S.-U., Song, C.-K., 2005. A simple semi-empirical photochemical model for the simulation of ozone concentration in the Seoul metropolitan area in Korea. Atmos. Environ. 39 (30), 5597–5607. https://doi.org/10.1016/j.atmosenv.2005.06.016.

Kim, H., Gil, J., Lee, M., Jung, J., Whitehill, A., Szykman, J., Lee, G., Kim, D.-S., Cho, S., Ahn, J.-Y., Hong, J., Park, M.-S., 2020. Factors controlling surface ozone in the Seoul metropolitan area during the KORUS-AQ campaign. Elem. Sci. Anth. 8, 46. https://doi.org/10.1525/elementa.444.

Kleist, E., Mentel, T.F., Andres, S., Bohne, A., Folkers, A., Kiendler-Scharr, A., Rudich, Y., Springer, M., Tillmann, R., Wildt, J., 2012. Irreversible impacts of heat on the emissions of monoterpenes, sesquiterpenes, phenolic BVOC and green leaf volatiles from several tree species. Biogeosciences 9, 5111–5123. https://doi.org/10.5194/bg-9-5111-2012.

Laothawornkitkul, J., Taylor, J.E., Paul, N.D., Hewitt, C.N., 2009. Biogenic volatile organic compounds in the Earth system. New Phytol. 183 (1), 27–51. https://doi.org/10.1111/j.1469-8137.2009.02859.x.

Lee, H.-J., Chang, L.-S., Jaffe, D.A., Bak, J., Liu, X., Abad, G.G., Jo, H.-Y., Jo, Y.-J., Lee, J.-B., Kim, C.-H., 2021. Ozone continues to increase in East Asia despite decreasing NO2: causes and abatements. Remote Sens. 13 (11), 2177. https://doi.org/10.3390/rs13112177.

Lee, H.-J., Chang, L.-S., Jaffe, D.A., Bak, J., Liu, X., Abad, G.G., Jo, H.-Y., Jo, Y.-J., Lee, J.-B., Yang, G.-H., Kim, J.-M., Kim, C.-H., 2022. Satellite-based diagnosis and numerical verification of ozone formation regimes over nine megacities in East Asia. Remote Sens. 14 (5), 1285. https://doi.org/10.3390/rs14051285.

MOE (Ministry of Environment) (Korea), 2019. Heatwave risk in Korea is expected to increase further over the next 10 years [press release]. https://www.me.go.kr/home/web/board/read.do?boardId=1026705&boardMasterId=1.

Oak, Y.J., Jacob, D.J., Pendergrass, D.C., Dang, R., Colombi, N.K., Chong, H., Lee, S., Kuk, S.K., Kim, J., 2025. Air quality trends and regimes in South Korea inferred from 2015–2023 surface and satellite observations. Atmos. Chem. Phys. 25 (5), 3233–3252. https://doi.org/10.5194/acp-25-3233-2025.

Oh, I.-B., Kim, Y.-K., Lee, H.W., Kim, C.-H., 2006. An observational and numerical study of the effects of the late sea breeze on ozone distributions in the Busan metropolitan area, Korea. Atmos. Environ. 40 (7), 1284–1298. https://doi.org/10.1016/j.atmosenv.2005.10.049.

Palmer, P.I., Jacob, D.J., Fiore, A.M., Martin, R.V., Chance, K., Kurosu, T.P., 2003. Mapping isoprene emissions over North America using formaldehyde column observations from space. J. Geophys. Res. Atmos. 108 (D6), 4180. https://doi.org/10.1029/2002JD002153.

Peñuelas, J., Staudt, M., 2010. BVOCs and global change. Trends Plant Sci. 15 (3), 133–144. https://doi.org/10.1016/j.tplants.2009.12.005.

Pu, X., Wang, T.J., Huang, X., Melas, D., Zanis, P., Papanastasiou, D.K., Poupkou, A., 2017. Enhanced surface ozone during the heat wave of 2013 in Yangtze River Delta region, China. Sci. Total Environ. 603–604, 807–816. https://doi.org/10.1016/j.scitotenv.2017.03.056.

Pusede, S.E., Steiner, A.L., Cohen, R.C., 2015. Temperature and recent trends in the chemistry of continental surface ozone. Chem. Rev. 115 (10), 3898–3918. https://doi.org/10.1021/cr5006815.

Rasmussen, D.J., Hu, J., Mahmud, A., Kleeman, M.J., 2013. The ozone–climate penalty: past, present, and future. Environ. Sci. Technol. 47 (24), 14258–14266. https://doi.org/10.1021/es403446m.

Vautard, R., Honoré, C., Beekmann, M., Rouil, L., 2005. Simulation of ozone during the August 2003 heat wave and emission control scenarios. Atmos. Environ. 39 (16), 2957–2967. https://doi.org/10.1016/j.atmosenv.2005.01.039.

Weaver, C.P., Liang, X.-Z., Zhu, J., Adams, P.J., Amar, P., Avise, J., Caughey, M., Chen, J., Cohen, R.C., Cooter, E., Dawson, J.P., Gilliam, R., Gilliland, A., Goldstein, A.H., Grambsch, A., Grano, D., Guenther, A., Gustafson, W.I., Harley, R. A., et al., 2009. A preliminary synthesis of modeled climate change impacts on U.S. regional ozone concentrations. Bull. Am. Meteorol. Soc. 90 (12), 1843–1863. https://doi.org/10.1175/2009BAMS2568.1.

Wells, K.C., Millet, D.B., Payne, V.H., Deventer, M.J., Bates, K.H., de Gouw, J.A., Graus, M., Warneke, C., Wisthaler, A., Fuentes, J.D., 2020. Satellite isoprene retrievals constrain emissions and atmospheric oxidation. Nature 585 (7824), 225–233. https://doi.org/10.1038/s41586-020-2664-3.

Wie, J., Moon, B.-K., Hyun, Y.-K., Lee, J., 2021. Impact of local atmospheric circulation and sea surface temperature of the East Sea on heat waves over the Korean Peninsula. Theor. Appl. Climatol. 144 (1–2), 431–446. https://doi.org/10.1007/s00704-021-03546-8.

Wiedinmyer, C., Guenther, A., Harley, P., Hewitt, N., Geron, C., Artaxo, P., Steinbrecher, R., Rasmussen, R., 2004. Global organic emissions from vegetation. In: Granier, C., Artaxo, P., Reeves, C.E. (Eds.), Emissions of Atmospheric Trace Compounds. Kluwer Academic Publishers, pp. 115–170. https://doi.org/10.1007/978-1-4020-2167-1.

Woo, J.-H., Choi, K.-C., Kim, H.K., Baek, B.H., Jang, M., Eum, J.-H., Song, C.H., Ma, Y.-I., Sunwoo, Y., Chang, L.-S., Yoo, S.H., 2012. Development of an anthropogenic emissions processing system for Asia using SMOKE. Atmos. Environ. 58, 5–13. https://doi.org/10.1016/j.atmosenv.2011.10.042.

Woo, J.-H., Kim, Y., Kim, H.-K., Choi, K.-C., Eum, J.-H., Lee, J.-B., Lim, J.-H., Kim, J., Seong, M., 2020. Development of the CREATE inventory in support of integrated climate and air quality modeling for Asia. Sustainability 12 (19), 7930. https://doi.org/10.3390/su12197930.

Wu, Y., Zheng, Z., Chen, X., Zhong, W., Yuan, X., Zhong, W., Lei, R., Li, C., Zhuang, Y., Gao, X., Li, X., Lin, H., Chen, L., Cai, W.-J., Qi, D., 2025. Amplified warming accelerates deoxygenation in the Arctic Ocean. Nat. Clim. Change 15 (8), 859–865. https://doi.org/10.1038/s41558-025-02376-0.

Zhao, K., Bao, Y., Huang, J., Wu, Y., Moshary, F., Arend, M., Wang, Y., Lee, X., 2019. A high-resolution modeling study of a heat wave-driven ozone exceedance event in New York City and surrounding regions. Atmos. Environ. 199, 368–379. https://doi.org/10.1016/j.atmosenv.2018.10.059.

Zhou, Y., Guan, H., Huang, C., Fan, L., Gharib, S., Batelaan, O., Simmons, C., 2019. Sea breeze cooling capacity and its influencing factors in a coastal city. Build. Environ. 166, 106408. https://doi.org/10.1016/j.buildenv.2019.106408.